Journal of Membrane Science and Research 6 (2020) 147-157

Journal of Membrane Science & Research

journal homepage: www.msrjournal.com

Research Paper

Synthesis of Calcium Fluoride Ultrafine Particles for the Preparation of Integral Asymmetric Cellulose Acetate/Calcium Fluoride Membranes

Andrea Molina Estrada [1], Mónica Faria [2], Gladis Judith Labrada Delgado [3], Maria Norberta de Pinho [2,*], María Guadalupe Sánchez Loredo [1]

[1] *Instituto de Metalurgia, Universidad Autónoma de San Luis Potosí, Sierra Leona 550, 78210 San Luis Potosí, S.L.P., Mexico*
[2] *CeFEMA and Department of Chemical Engineering, Universidade de Lisboa - Instituto Superior Técnico, Av. Rovisco Pais, 1049-001 Lisbon, Portugal*
[3] *Instituto Potosino de Investigación Científica y Tecnológica, Camino a la Presa San José 2055, 78216 San Luis Potosí, Mexico*

Article info

Received 2019-12-19
Revised 2020-02-18
Accepted 2020-02-22
Available online 2020-02-22

Keywords

Composite membranes
Fluorite
Cellulose acetate
Integral asymmetric membranes
Solvent evaporation method
Ultrafiltration

Graphical abstract

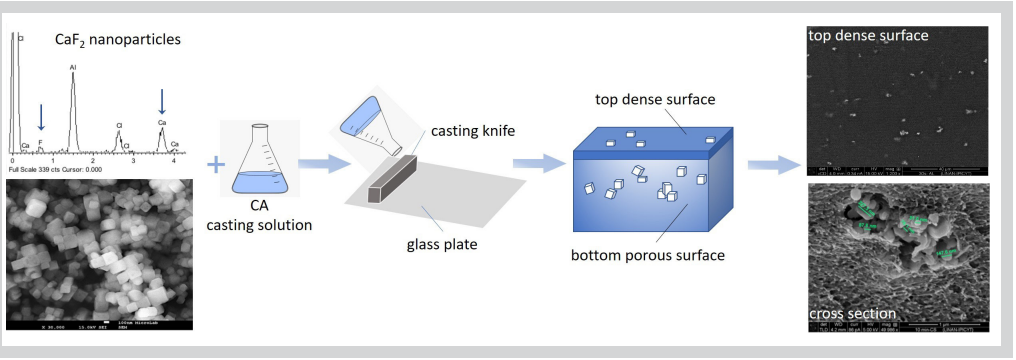

Highlights

- Synthesis of fluorite fine particles by a double jet injection method
- Synthesis of novel composite membranes containing a highly hydrophilic filler
- Fluorite particles influence structure and therefore permeation properties
- Incorporation of fluorite nanoparticles increase hydraulic permeability

Abstract

The present work reports on the synthesis of cellulose acetate (CA) asymmetric membranes with the incorporation of inorganic fluorides, CaF_2 particles. These fillers of polymeric composites can, according to the literature, promote the ordering of the polymer matrix, which can lead to interesting permeation properties. In order to achieve that, fluorite (CaF_2) fine particles were prepared by a double jet injection method using $CaCl_2$ and NaF solutions as precursors and polyvinylpyrrolidone as a stabilizing agent. The fluorite particles were incorporated in the casting solutions of cellulose acetate/acetone/formamide. Dynamic light scattering measurements showed that formamide acting as the poor solvent in the membrane casting solutions can lead to some agglomeration of the fluorite particles and evident changes in structure and permeation properties. The CA/CaF_2 composite membranes were casted by the phase inversion method at different solvent evaporation times. The permeation experiments indicated that the active layer of the membranes prepared with shorter solvent evaporation times is composed of an organic-inorganic network with bigger pores, which allows the permeation of molecules approximately two times the size of those retained by the CA membranes. Further increase in the solvent evaporation time has the opposite effect, as particle agglomerates may be formed.

1. Introduction

The purpose of blending inorganic fillers into different polymer matrices is usually the improvement of polymeric materials' performance. Since the properties depend on the structural features of the polymeric composite, they depend greatly on the dispersion and orientation of the fillers in the matrix, as well as on their interaction with the polymer [1,2].

Ceramic fine particles are materials possessing outstanding chemical and thermal resistances, and they are interesting as fillers in polymeric composites not only because of these features, but also because they are easily obtained at a relatively low cost. Among these ceramic fine particles, calcium fluoride, when used as a filler in composite materials, is attractive due to its high optical transparence in a broad wavelength range (from vacuum ultraviolet to mid-infrared), low phonon energy, high chemical resistance, thermal conductivity, dielectric properties, low cost, and biocompatibility [1–7]. As far as we know, few works report on the modification of polymers using inorganic fluorides, in spite of the fact that CaF_2 particles would be interesting components of polymeric composites, since they can act as nucleating agents accelerating the crystallization of the polymer matrix and they enhance the thermal properties and adjust the surface and optical properties of the composites [1–5]. Nanosized CaF_2 as a filler in membrane fabrication could confer more chemical and mechanical resistance to the polymers and, perhaps even more important, antibacterial properties that would extend the life of membranes usually prone to biofilm formation and fouling. The bactericide

* Corresponding author: marianpinho@tecnico.ulisboa.pt (M.N. de Pinho)

DOI: 10.22079/JMSR.2020.118838.1314

properties of CaF_2 have been reported on [6] and the combination of fluorite and other reagents has proven to improve dental treatments protecting teeth against cariogenic microorganisms [8,9].

In the past, research has been focused on the properties and performance of polymeric cellulose acetate (CA) [10] and monophasic hybrid CA/silica [11,12] integral asymmetric membranes. Despite the huge amount of work concerning these polymeric membranes, the modification of the basic characteristics of CA using fluoride-based materials as fillers has been rarely reported.

The present work addresses the innovative synthesis of CaF_2 nanoparticles by the double-jet precipitation technique which was adapted from the method used by Safronikhin et al. [13] for the preparation of LaF_3 nanoparticles. The CaF_2 nanoparticles are thoroughly characterized by X-ray diffraction (XRD), transmission electron microscopy (TEM) and dynamic light scattering (DLS). The second part of the study reports on the synthesis of CA/CaF_2 composite integral asymmetric membranes by incorporation of the CaF_2 nanoparticles into cellulose acetate/formamide/acetone casting solutions with 17/30/53 (wt.%) compositions. The surface and structure properties of the CA/CaF_2 composite membranes are studied, the permeation performance is assessed in terms of hydraulic permeability, and the molecular weight cut-off (MWCO) is estimated through the determination of the rejection coefficients to organic solutes with increasing molecular weights.

2. Experimental

2.1. Materials and chemicals

Cellulose acetate (CA) (Sigma-Aldrich, ~30,000 g/mol), formamide (Sigma-Aldrich, >99.5% purity), acetone (Labchem, 99.9% purity), sodium fluoride (NaF) (Merck, >99.5% purity), polyvinylpyrrolidone (PVP) (~44.000 g/mol, >88.18%, BDH Chem.), sodium chloride (NaCl) (VWR, 99.9% purity), calcium chloride ($CaCl_2.2H_2O$) (Merck, 99.0% purity), sodium sulfate (Na_2SO_4) (Scharlau, 99% purity), magnesium chloride hexahydrate ($MgCl_2.6H_2O$) (Riedel-de Haen, 99%), magnesium sulfate heptahydrate ($MgSO_4.7H_2O$) (Merck, 99.5%), magnesium perchlorate ($Mg(ClO_4)_2$), potassium chloride (KCl) (Merck, 99.5%), and potassium sulfate (K_2SO_4) (Scharlau, 99.5%). D(þ)-Glucose anhydrous (PA-ACS) (Panreac), Polyethylene glycol (PEG) PEG 1,000 Da (Merck), PEG 10,000 Da (Merck), Dextran 70,000 Da (Pharmacia), and Dextran 110,000 Da (Pharmacia).

2.2. Synthesis of CaF_2 ultrafine particles

In a typical experiment, reagent solutions were prepared by dissolving 0.6086 g $CaCl_2.2H_2O$ in 25 mL of a 20 g/L PVP solution, and 0.2624 g NaF in another 25 mL of the same PVP solution. Both solutions were simultaneously added dropwise into 25 mL of a 20 g/L PVP solution at 25 ºC under vigorous stirring. When the addition of the reagents was finished, the system was kept under stirring for 10 minutes. The product was separated by adding NaCl to precipitate the particles, followed by centrifugation at 11,000 rpm for 10 minutes. The solid was washed six times with water and twice with acetone.

2.3. Characterization of CaF_2 ultrafine particles

Phase analysis and crystallinity determination of synthesized CaF_2 material were conducted by powder X-ray diffraction (XRD) using a Bruker D8 Advance Diffractometer (Cu Kα radiation, λ = 1.54060 Å; 40 kV, 35 mA, Instituto de Metalurgia/UASLP). The XRD data were collected in the 2-hour range from 4 to 90° 2theta, with a step size of 0.02° and a counting time of 3.35 s. The characterization was performed on a dried powder sample, which was obtained by precipitation of the nanoparticles, adding acetone to the aqueous dispersion and washing with water and isopropanol. XRD analysis was carried out using a silicon single crystal ((911) orientation) as sample holder to minimize scattering. To estimate the average crystallite size and specific crystallite size anisotropy from diffraction peak broadening reflections (using the Scherrer equation), the Rietveld refinement (Le Bail method) was performed using the Bruker software TOPAS 4.2. For each Rietveld refinement, the instrumental correction was included as determined, with a standard powder sample Al_2O_3 (from National Institute of Standards and Technology (NIST)) as standard reference material, NIST 1976a). The diffraction pattern was analyzed qualitatively using the PDF-2 (2010) of ICDD databases.

The particle size of CaF_2 particles was determined by transmission electron microscopy (TEM). Images were acquired using a Hitachi H-7000 microscope (Japan) with an 80 kV acceleration voltage. The samples were prepared by depositing a droplet of a diluted colloid suspension of the particles onto a holey carbon Formvar filmed grid and allowing the solvent (ethanol) to evaporate. Dynamic light scattering (DLS) measurements were performed using a Zetasizer NanoRange (Malvern). The particles were suspended in the solvents used in the casting solutions. The concentration of the particles in the suspension was 10 ppm. Six measurements were taken for each sample at a temperature of 25 °C.

2.4. Membrane preparation

Flat sheet membranes were prepared by the phase inversion method [14]. The cellulose acetate (CA) flat sheet membranes, referred to as CA membranes, were cast from casting solutions containing CA, acetone and formamide. The CA/CaF_2 composite membranes were obtained from the incorporation of CaF_2 nanoparticles into the casting solutions to yield the CA/CaF_2 membranes. The casting solution composition and casting conditions are presented in Table 1. The solvent evaporation time, in minutes, is added to the membrane designation. To prepare the casting solutions of the composite membranes, the CaF_2 nanoparticles were introduced in the acetone solution. The casting solutions were subjected to stirring in a mechanical shaker (Vibromatic, Selecta) for approximately 24 hours. The casting solutions were spread on a clean glass plate using a casting knife of 250 µm. The glass plate was left in contact with the air for the duration of the solvent evaporation step, after which it was immersed in ice cold water for 2 hours.

Table 1
Casting solution composition and film casting conditions of CA and CA/CaF_2 membranes.

	CA membranes			**CA/CaF_2 composite membranes**		
Casting solution (wt.%)	**CA0.5**	**CA2**	**CA10**	**CA/$CaF_2$0.5**	**CA/$CaF_2$2**	**CA/$CaF_2$10**
Cellulose Acetate	17.00			16.98		
Formamide	30.00			29.97		
Acetone	53.00			52.95		
CaF_2	-			0.10		
Casting conditions						
Solvent evaporation time (min)	0.5	2.0	10.0	0.5	2.0	10.0
Solution temperature (ºC)	20-25					
Atmosphere's temperature (ºC)	20-25					
Gelation medium	water at 0 ºC for 2h					

2.5. Surface and structure properties of Cellulose Acetate/CaF_2 membranes

The active layer surfaces, the porous layer bottom surfaces, and the cross-sections of the CA membranes and the composite CA/CaF_2 membranes described in Table 1 were observed by Field Emission Scanning Electron Microscopy (FESEM, JM-7001F FEG-SEM, JEOL). Prior to being imaged by SEM, the CA/CaF_2 membranes were submitted to a drying process previously described [11]. SEM characterization with the Backscattered Electron (BSE) Detector was carried out using first an ESEM-FEG-Quanta 250, Thermo-Fisher Scientific. In order to obtain more information on the particle distribution in the active layer and cross-section of the membranes, the BSE detector for atomic contrast analysis, in a brand double-beam scanning electron microscope FEI-Helios Nanolab 600 (IPICyT) was used. Characterization by means of atomic contrast was carried out only for the membranes with embedded particles. The membranes were dried at room temperature, fractured in liquid nitrogen, mounted on a stub and, then, sputter-coated with gold. All measurements, such as the active layer and overall membrane thickness, were obtained with the ImageJ version 1.4.3.67 (NIH Image, USA) software. A qualitative analysis was performed by means of X-ray energy dispersion spectrometry. This technique is based on the X-ray spectrum emitted by the solid sample, bombarded by a focused electron

beam, obtaining a localized chemical analysis. This analysis was done in specific areas where CaF_2 nanoparticles were observed by means of FESEM.

2.6. Permeation experiments

The permeations experiments were performed in a crossflow filtration set-up that has been previously described [15]. Briefly, it consists of six flat plate cells with two detachable parts separated by a porous support plate, each of which holds a membrane with a total surface area of 13.2 cm^2. Other components of the experimental set-up include a feed tank, a pump, a flowmeter, two manometers, and a pressure control valve. Prior to every permeation experiment, the membranes were compacted for 3 hours at 3 bar and a flow rate of 180 L/h in order to avoid pressure effects on the membrane structure in subsequent experiments. The membranes were characterized by the hydraulic permeability (L_p) which was obtained by the slope of the straight line fitted to the water permeate fluxes (J_{pw}) as a function of the transmembrane pressure (ΔP), being, therefore, $L_p = \frac{J_{pw}}{\Delta P}$.

The separation performance of the CA and CA/CaF_2 membranes was determined in terms of the apparent rejection coefficients towards organic solutes of increasing molecular weight: glucose, PEG 1000, PEG 10000, Dextran 70000, and Dextran 110000. The apparent rejection coefficients (f) are defined as $f = \frac{C_f - C_p}{C_f}$, where C_f and C_p are the solute concentrations in the bulk of the feed solution and of the permeate solution, respectively. All experiments were conducted individually for one solute with an initial feed concentration of 2 g/L, a feed pressure of 3 bar and a feed flow rate of 180 L/h after a stabilization time of 30 minutes. The organic compound concentrations were determined in terms of total organic carbon (TOC) content by a Dohrmann Total Organic Carbon Analyzer Model DC-85A.

The molecular weight cut-off (MWCO) of the CA and CA/CaF_2 membranes is estimated through the determination of the rejection coefficients to the organic solutes (glucose, PEG 1,000 Da, PEG 10,000 Da, Dextran 70,000 Da, Dextran 110,000 Da). The MWCO value is obtained by the intersection of the curve of $\log\frac{f}{1-f}$ vs MW with the straight line of $\log\frac{f}{1-f}$ =1 which corresponds to a rejection coefficient of f = 90.9%.

3. Results and discussion

3.1. Synthesis and characterization of CaF_2 ultrafine particles

Figure 1 shows the XRD patterns of the powders of CaF_2 nanoparticles synthesized in water containing PVP as stabilizer. PVP act as a capping agent in nanoparticle synthesis. PVP surrounds the particle and naturally restricts it from growing and aggregating. When using polymers as protecting agents in nanoparticle synthesis, the steric forces keep the particles, which have a high surface energy because of their small size, separated from each other, preventing agglomeration. On the other hand, minimizing filler aggregation during composite preparation is also an important consideration [1,2]. To ensure this, chemical modification of the surface of the inorganic filler particles to provide chemical compatibility and improve the dispersion in the polymer matrices is fundamental. The diffraction peaks can be well indexed to a cubic phase (fluorite-type structure) of CaF_2, space group Fm-3m (JCPDS No. 870971). Furthermore, in order to obtain detailed information about the composition, crystalline structure and mean size of the CaF_2 particles in the dispersion, a quantitative phase analysis of the diffraction patterns of the particles was performed using the computer program TOPAS [4.2]. The atomic positions were determined by Rietveld refinement (Table 2), obtaining a unit cell value of a = 5.46377(10) Å, assuming Fm-3m symmetry, and a crystallite size of 117.4 nm. For the fit of the sample, a Rwp value of 18.89% was obtained, Rp: 15.00, and GOF: 2.66.

Using the Miller indices (hkl) presented in Table 3, a value for a = 5.42 Å was obtained, close to the value reported in the literature, where a = 5.4355 Å [16], and the one obtained by means of Rietveld refinement.

TEM images in Figure 2 show that the CaF_2 sample consists mainly of cubic particles whereas the average crystallite size dXRD calculated from the Rietveld refinement is 117.4 nm, the particle size distribution obtained by TEM seems to be broader. There is a fundamental difference between the average crystallite sizes dXRD, calculated from XRD patterns, and the average particle sizes dTEM observed by TEM. The former is an average size of X-ray coherent scattering region of particles. The dXRD values are usually smaller than the average size values dTEM, calculated from the particle sizes observed by TEM. This can be attributed to the nonideality of real crystals (defects, differences in the chemical composition of the surface layer, etc.) and aggregation processes.

Table 2
Rietveld refinement of the CaF_2 fine particles.

Phase name	Fluorite			R-Bragg	4.899	
Space group	225			Scale	0.002068(14)	
Cell Mass	312.300			Cell Volume (≈^{3})	163.1083(91)	
Wt% - Rietveld	100.000			Crystallite Size (Cry Size Lorentzian, nm)	117.4(15)	
Crystal Linear Absorption Coef. (1/cm)	303.103(17)			Crystal Density (g/cm^3)		
Preferred Orientation (Dir 1: 022)	1(2400)			Lattice Parameter, a (≈)	5.46377(10)	
Site	Np	x	Y	Z	Atom Occ.	Beq
S1	4	0.00000	0.00000	0.00000	CA+2.1	0.41
S2	8	0.25000	0.25000	0.25000	F-1 1	0.62

Table 3
Miller indices (hkl) for CaF_2 crystals

Peak	(hkl)	Peak	(hkl)
1	(111)	4	(400)
2	(220)	5	(331)
3	(311)	6	(422)

FESEM characterization (Figure 3a) shows that the particles are apparently "encapsulated" by some organic reagent. EDS chemical analysis (Figure 3b) was used to prove the particles purity (taking into account the detection limit of the technique) and to check the efficiency of the washing steps (particularly the chlorides removal) before they were introduced in the casting solution. Finally, Figure 3c shows the particles after the washing steps. After these steps, the particles seem more defined and free of the film observed before washing. Figure 3c reveals particles whose diameter varies between 120-250 nm.

In order to obtain information about the compatibility of the particles and the solvents used for the preparation of the casting solution, a small amount of the CaF_2 particles was suspended in acetone, formamide, and a mixture corresponding to the proportions of acetone and formamide in the casting solution. The particle size distribution was studied using DLS (Figure 4) and showed that the particles agglomerated when suspended in formamide, but the presence of acetone in the casting solution helped avoid agglomeration to some extent. According to these results, formamide could act not only as a non-solvent during membrane formation, but also as a non-solvent for the filler, leading to changes in structure and, therefore, in permeation properties.

3.2. Structure and surface properties of Cellulose Acetate and Cellulose Acetate/CaF_2 membranes

The CA membranes and CA/CaF_2 composite membranes prepared with solvent evaporation times of 0.5, 2, and 10 minutes displayed an integral asymmetric structure. Figure 5 shows the SEM micrographs for the membranes casted with an evaporation time of 10 minutes. The first row (Figures 5a-c) pertains to the CA10 membrane while the second row (Figures 5d-f) shows micrographs of the CA/$CaF_2$10 composite membrane. Figures 5a and 5d show the surface morphology of the dense active layer, Figures 5b and e show the surface morphology of the bottom porous surface, and Figures 5c and f show the membrane cross-section structures.

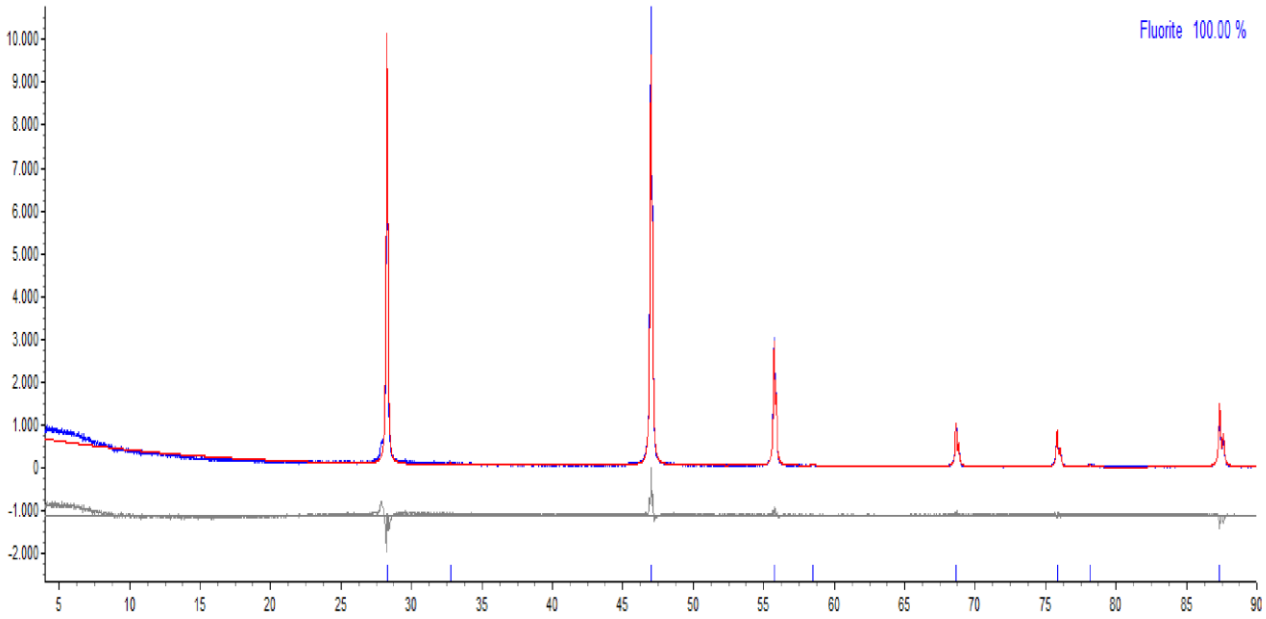

Fig. 1. Rietveld refined diffraction pattern of CaF_2.

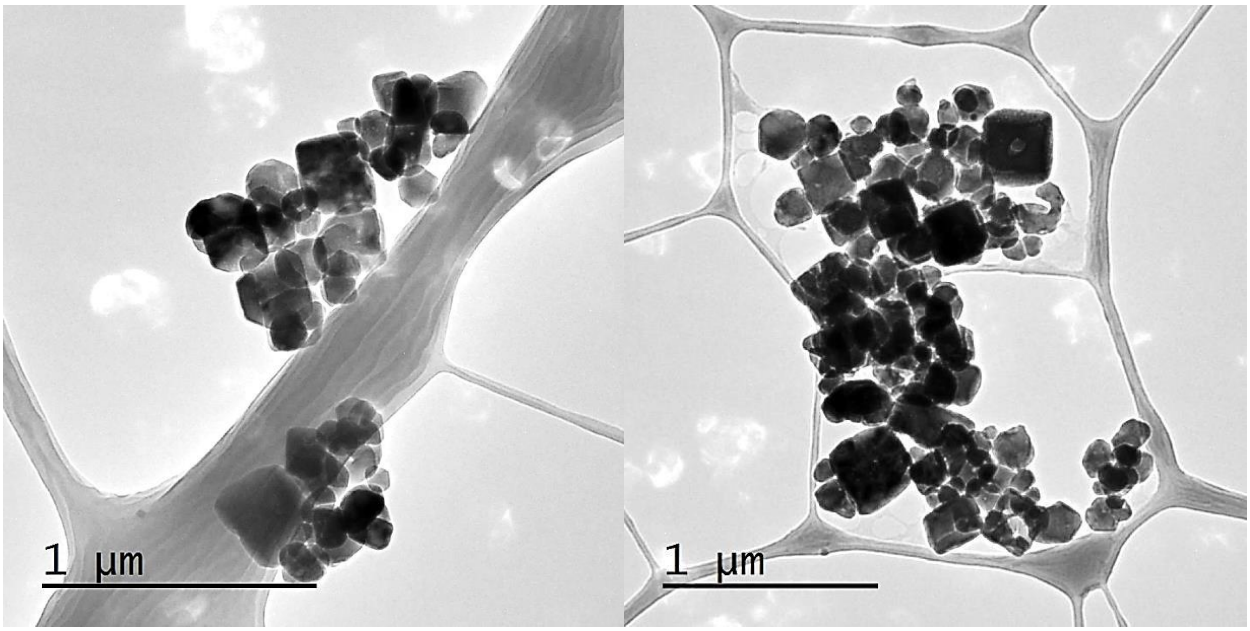

Fig. 2. Transmission electron micrography of calcium fluoride particles (as prepared).

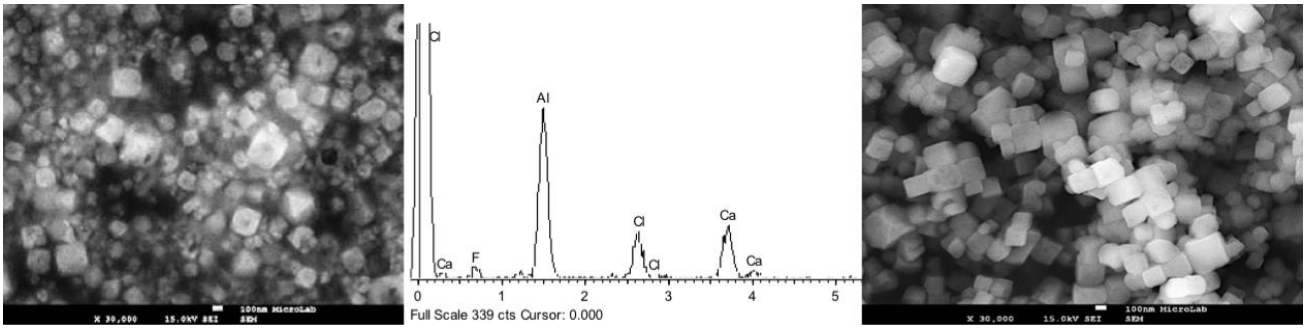

Fig. 3. (a) Scanning electron micrography of as-prepared CaF_2 particles, (b) EDS of calcium fluoride particles before washing, and (c) CaF_2 particles after the washing steps.

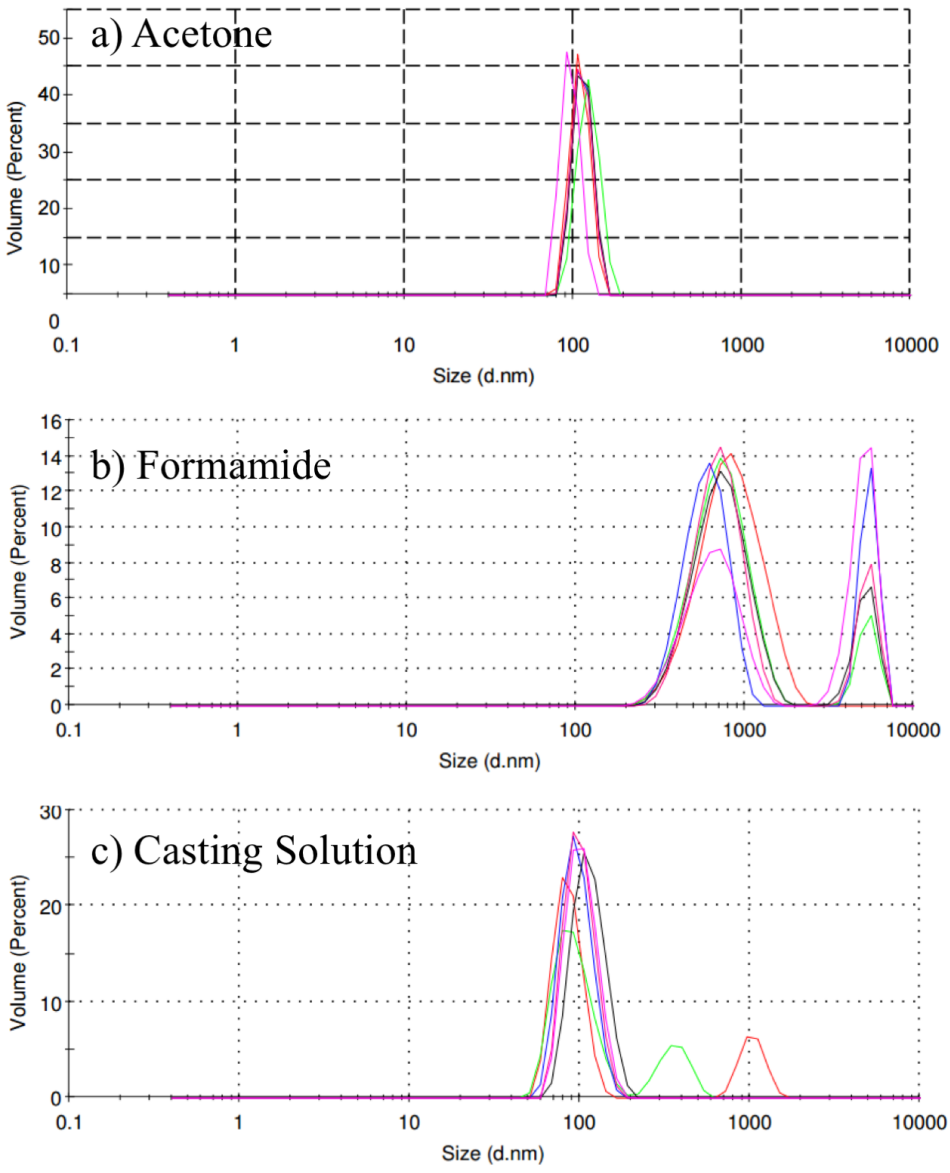

Fig. 4. Size distribution, obtained by DLS, of CaF_2 (a) suspended in acetone, (b) in formamide, (c) in a formamide-acetone mixture (36/64) corresponding to the casting solution; concentration of fluorite 10 ppm in all cases.

The asymmetric structure of the membranes is evident when observing the differences between the active layer (left column) and the porous layer (center column). The active layer has a smoother and pore-free surface while the bottom surface shows pore distribution. The images of the cross-sections are shown on the third column, where the presence of a dense active layer is evident at the top of the micrograph, with a significantly smaller thickness than the one on the bottom porous layer.

The FESEM images of the CA and CA/CaF_2 membranes prepared at evaporation times of 0.5 and 2 minutes are not presented as qualitatively they have identical surface and cross section morphologies as the ones represented in Figure 5 for an evaporation time of 10 minutes. However, a quantitative analysis using the ImageJ software reveals that the solvent evaporation time influences the thickness of the active layer and on the total thickness of the membranes. Table 4 shows these results obtained for the two sets of membranes, CA and CA/CaF_2, prepared at the three evaporation times. Comparing the overall thickness of the CA and CA/CaF_2 membranes, we can conclude that the membrane thickness increases with the increase in solvent evaporation time. Furthermore, as predicted, the active layer thickness of the CA membranes and of the composite CA/CaF_2 membranes also increases with the increase of the solvent evaporation time. An important observation is that the incorporation of CaF_2 nanoparticles in the membrane casting solutions influences both the overall thickness and the active layer thickness. For the three evaporation times, it is evident that the presence of CaF_2 decreases the active layer thickness of the membranes and that this reduction is more pronounced for the longer evaporation times of 2 and 10 minutes.

Figure 6b shows the EDS spectrum of the CA/$CaF_2$10 membrane cross-section and corresponds to the area marked in micrograph 6a. The spectrum reveals the presence of carbon, oxygen, calcium, and fluoride in the respective area. The carbon and oxygen elements can be attributed to the cellulose acetate of the polymeric matrix, and the inorganic elements represent CaF_2. For the CA/$CaF_2$0.5 and CA/$CaF_2$2 composite membranes, the EDS spectra revealed similar contributions from the carbon, oxygen, fluoride, and calcium elements, confirming the presence of CaF_2 fine particles.

Figure 7 shows the micrographs obtained from the CA/$CaF_2$10 membrane, where a region containing CaF_2 nanoparticles is circled in red. Figures 7b and c show amplifications of this region, where clusters of microparticles resembling nests are identified. Even though the particles show a significant degree of agglomeration, in Figures 7b and c the presence of uniform particles with sizes of ~100 nm can be identified. Similar clusters of particles were identified in the CA/$CaF_2$0.5 and CA/$CaF_2$2 composite membranes, indicating that the CaF_2 nanoparticles tend to arrange themselves in nest-like clusters throughout the cross-section structure of the polymer matrix.

Table 4
Active layer and total membrane thickness of the batch 1 CA membranes and CA/CaF_2 composite membranes.

	CA membranes			CA/CaF_2 composite membranes		
	CA0.5	**CA2**	**CA10**	**CA/$CaF_2$0.5**	**CA/$CaF_2$2**	**CA/$CaF_2$10**
Solvent evaporation time (min)	0.5	2.0	10.0	0.5	2.0	10.0
Membrane thickness (μm)	48	58	83	44	52	80
Active layer thickness (μm)	1.4	3.2	5.0	1.3	2.3	2.6

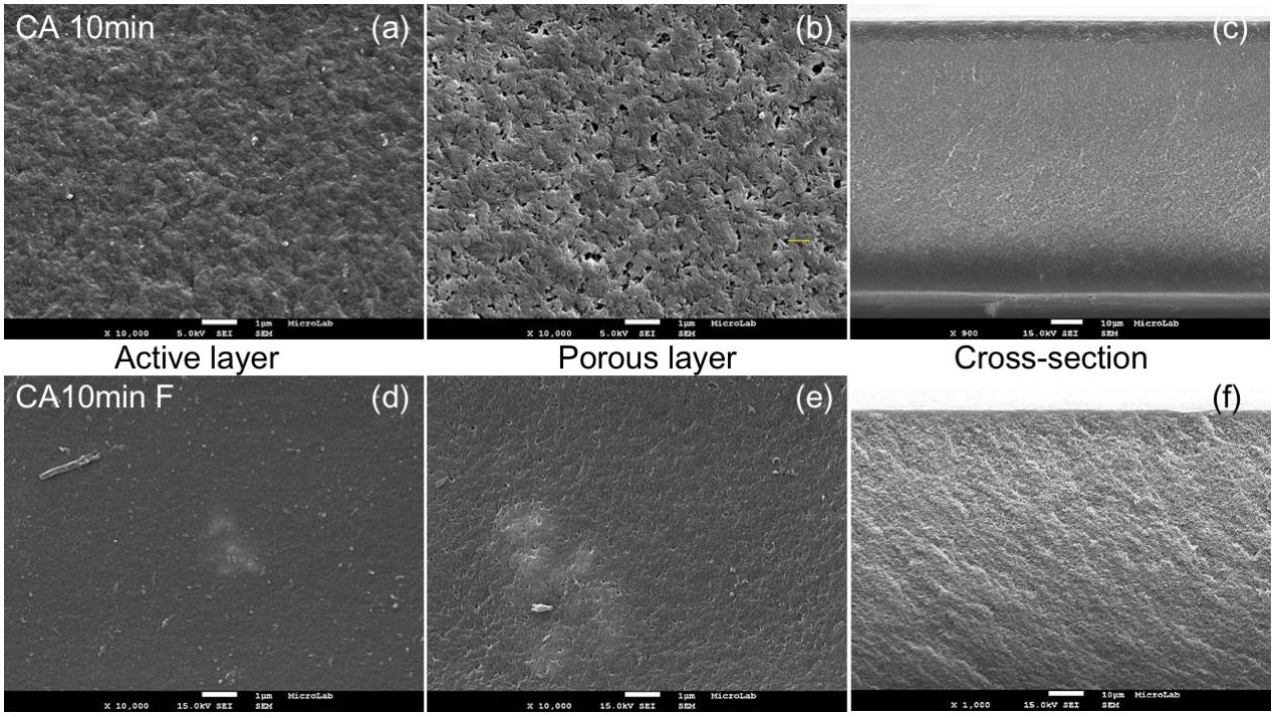

Fig. 5. SEM images (10,000x amplification) of the CA10 (first row) and CA/$CaF_2$10 (second row) membranes: a) and d) active layer dense surface, b) and e) porous surface, and c) and f) cross-section.

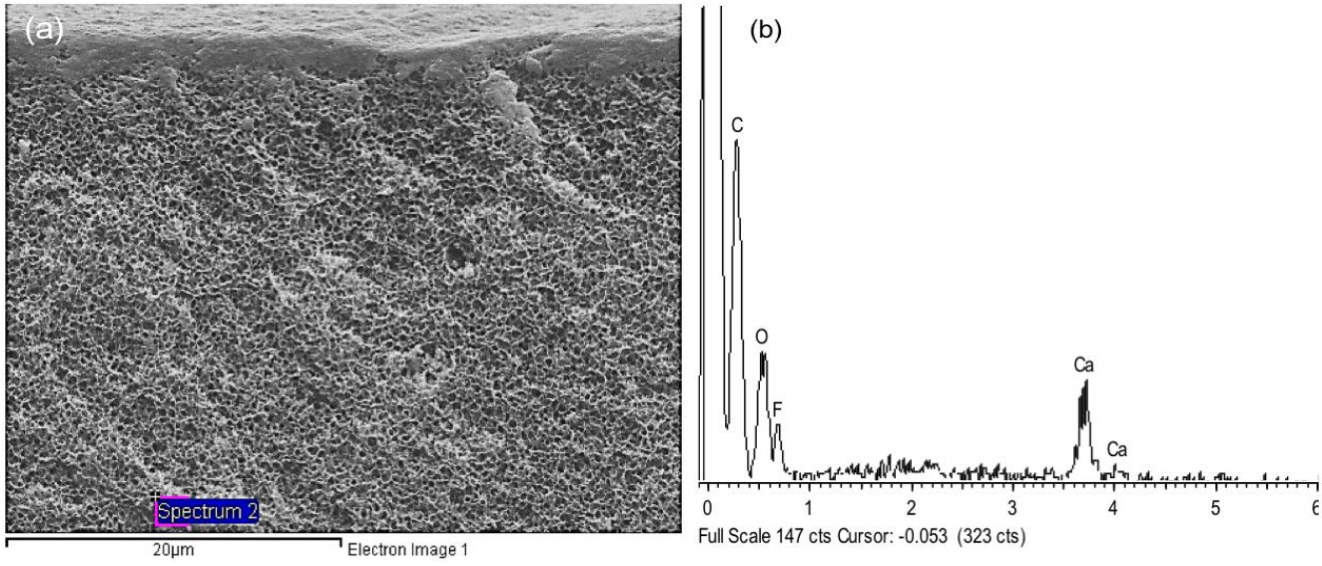

Fig. 6. (a) Cross-section micrograph of the CA/$CaF_2$10 membrane, (b) EDS spectrum of the area depicted in a purple square of the cross-section micrograph of the CA/$CaF_2$10 membrane containing 0.1% CaF_2.

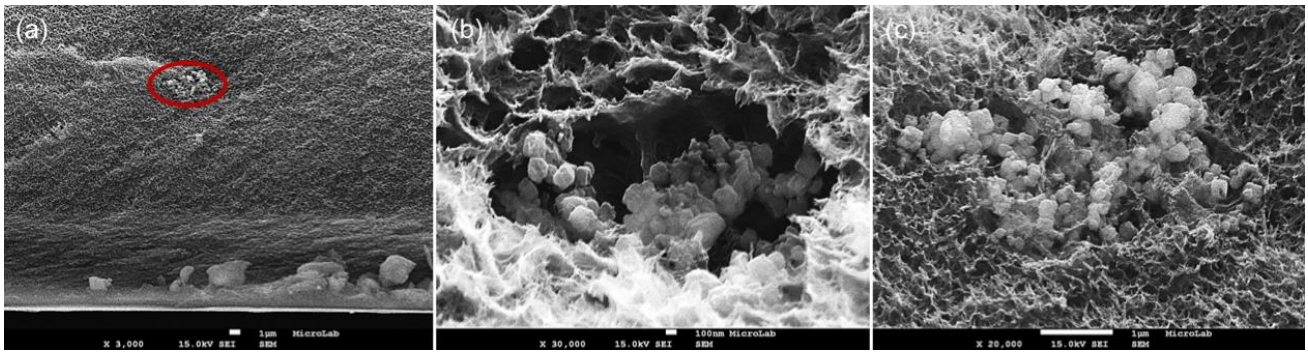

Fig. 7. (a) FESEM cross-section micrograph of the CA/$CaF_2$10 membrane with the area containing CaF_2 nanoparticles circled in red, (b) FESEM micrograph with 30,000x amplification, and (c) 20,000x amplification of the area circled in (a).

To obtain more information on the particle distribution in the membranes, particularly in the active layer and in the cross-section of the membranes, and on the interaction of the fillers with the polymeric matrix, both the secondary and the backscattering electron detectors were used. Figure 8 shows the micrographs taken for the characterization of the CA/$CaF_2$0.5, CA/$CaF_2$2, and CA/$CaF_2$10 membranes. The backscattering detector is particularly effective in identifying irregular particles, which appear as bright spots in the images (at low magnifications). This is because both atoms which compose these CaF_2 irregular particles have an atomic number higher than carbon, which is the main constituent of the polymer matrix.

Figure 8a shows the active layer and the bright spots corresponding to the filler on top and a small agglomerate composed of several particles. Figures 8b and c show micrographs of the CA/$CaF_2$2 and CA/$CaF_2$10 membranes' cross-sections. Both micrographs show fine fluorite particles, but only the particles in the CA/$CaF_2$2 membrane seem to be integrated in the polymer matrix. Figures 8d-f show cross-sections of the CA/$CaF_2$0.5, CA/$CaF_2$2, and CA/$CaF_2$10 membranes at different magnifications. In the CA/$CaF_2$0.5 membrane, the filler particles are difficult to identify and a clear border between active and porous layer is evident. The CA/$CaF_2$2 membrane shows bright zones corresponding to aggregates of CaF_2. Figure 8f shows a membrane possessing an irregular surface, and one can observe again the cluster of particles resembling nests and a very porous support layer.

Figure 9 shows the micrographs with secondary (9a) and backscattered electron detectors of the CA/$CaF_2$0.5, CA/$CaF_2$2, and CA/$CaF_2$10 membranes. The difference between the images obtained using the two detectors is evident, since Figures 9b-d show "bright spots" which refer to an atomic number greater than that of the matrix, corresponding to CaF_2. Particle dispersion is not ideal, since agglomerates are clearly observed; however, it appears that most are located in the active layer, which could lead to changes in permeation properties. Smaller, non-aggregate particles are also observed.

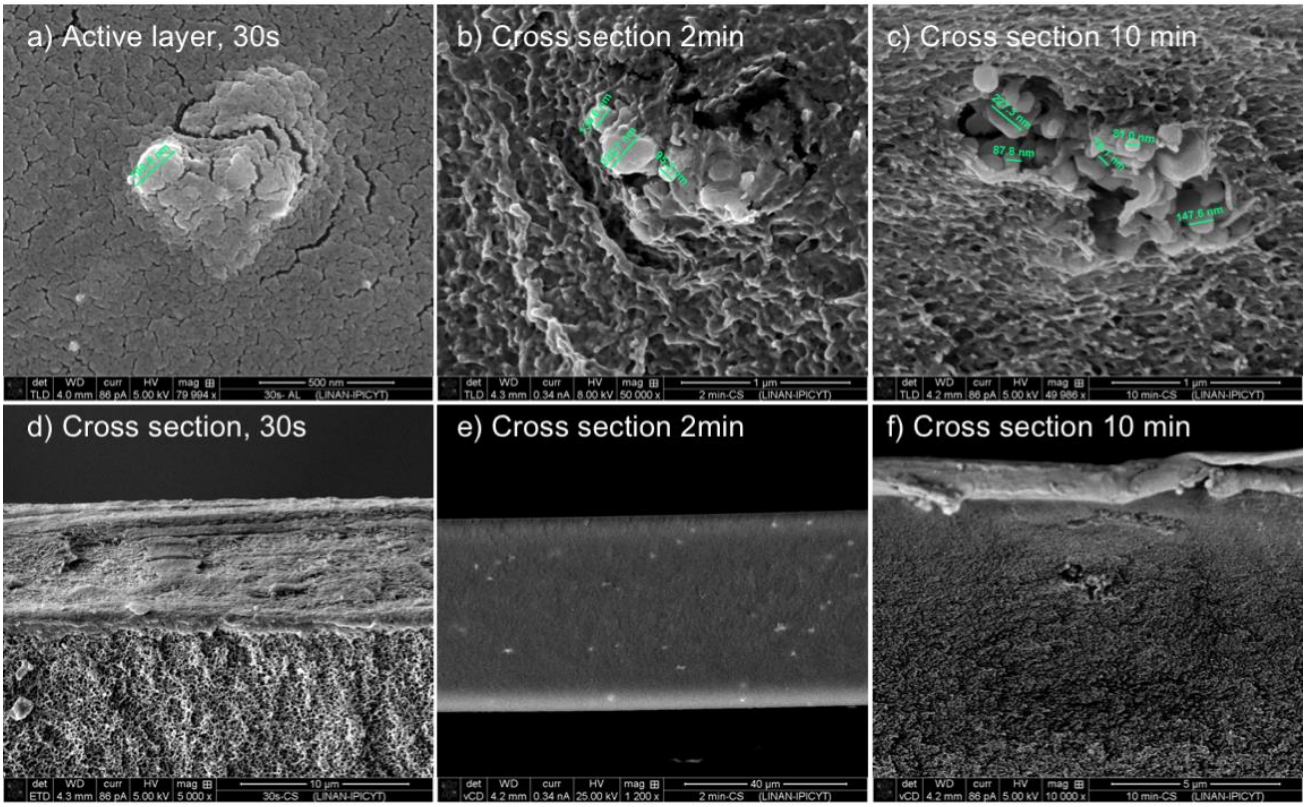

Fig. 8. Micrographs of the CA/$CaF_2$0.5, CA/$CaF_2$2, and CA/$CaF_2$10 membranes.

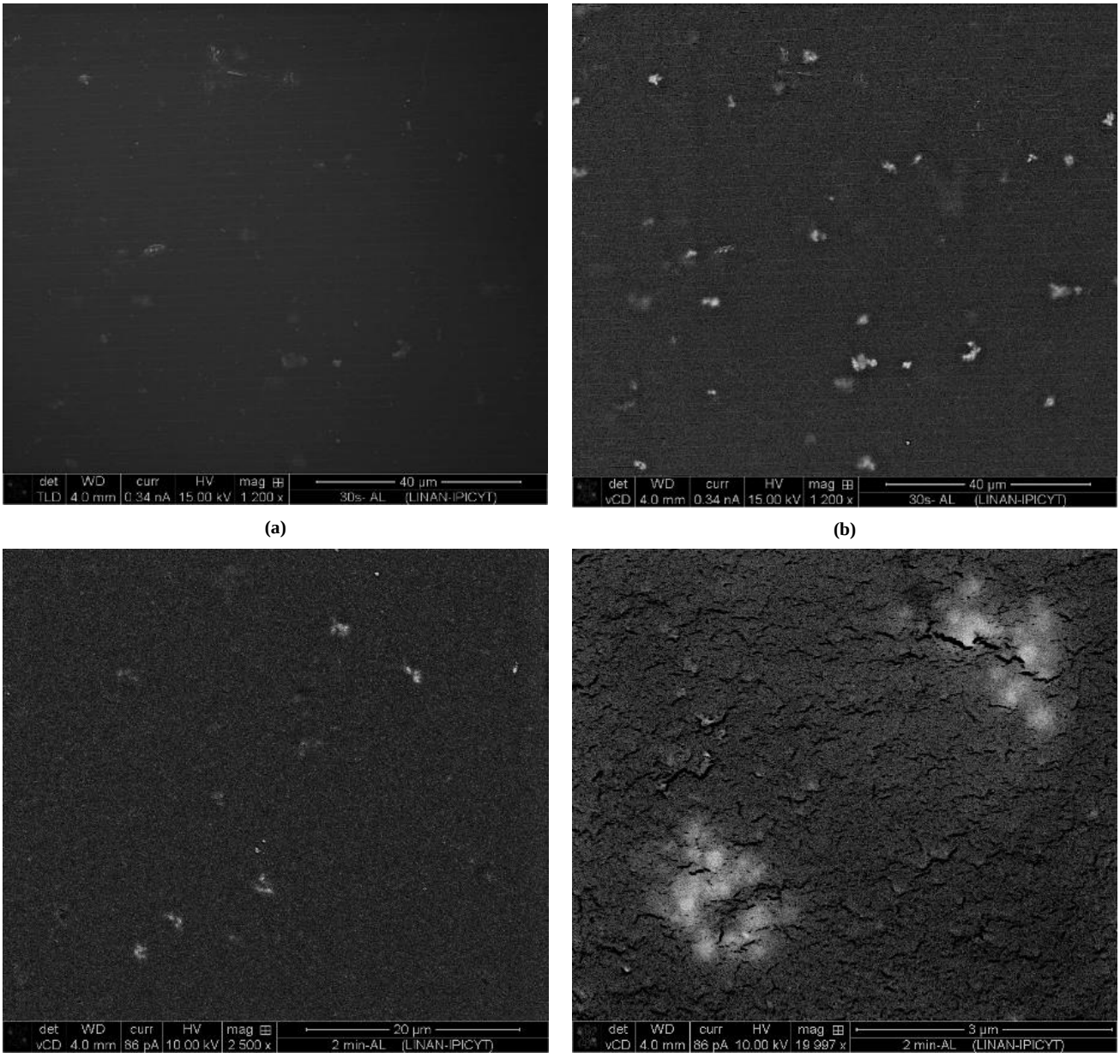

Fig. 9. Active layer micrograph of the CA/$CaF_2$0.5 membrane taken using a) the secondary detector, b) the backscattered electron detector, CA/$CaF_2$2, c) and d) the backscattered electron detector of the CA/$CaF_2$10 membrane.

3.3. Permeation properties of the Cellulose Acetate/CaF_2 membranes

Figure 10 shows the variation of the pure water permeation fluxes vs the transmembrane pressure for the CA and CA/CaF_2 composite membranes. The hydraulic permeability, L_p, is given by the slope of the straight lines in Figure 10. The values of L_p are 45, 14, and 12 $kgm^{-2}h^{-1}bar^{-1}$ for the CA0.5, CA2, and CA10 membranes, respectively, whereas the L_p values are 48, 19, and 18 $kgm^{-2}h^{-1}bar^{-1}$ for the CA/$CaF_2$0.5, CA/$CaF_2$2, and CA/$CaF_2$10 membranes, respectively.

It is well known that, in the synthesis of integral asymmetric membranes by the phase inversion method, the increase of the solvent evaporation time leads to the increase of the active layer thickness and, therefore, to the increase of the resistance to water permeation and the decrease of the hydraulic permeability. In fact, as Figure 11 shows, the permeability, L_p, decreases with the increase of the active layer thickness (see Table 4) for both the CA and the CA/CaF_2 composite membranes. This effect is more pronounced when the solvent evaporation time increases from 2 to 10 minutes. The incorporation of the CaF_2 particles leads to a significant increase in the hydraulic permeability of the CA/CaF_2 membranes. For the solvent evaporation time of 10 minutes, the incorporation of the ceramic particles reflects an increase in permeability from 12 to 18 $kgm^{-2}h^{-1}bar^{-1}$.

The selective permeation to the organic solutes – glucose, PEG 1,000 Da, PEG 10.000 Da, Dextran 70,000 Da, Dextran 110,000 Da – is given by the rejection percentages displayed in Figure 12. The two smaller solutes – glucose and PEG 1000 – have rejection coefficients below 40% for all the membranes. The high rejection coefficients to the three solutes with increasing molecular weights of 10,000, 70,000, and 110,000 Da are used in the graphical representation described in Section 2.5 to yield the molecular weight cut-off (MWCO) of the membranes. Figure 13 displays that the CA10 membrane yields a MWCO of 70 000 Da.

In terms of the MWCO, the incorporation of 0.05 wt.% of CaF_2 doubles the value of the MWCO in the membranes prepared with a solvent evaporation time of 0.5 and 2 min: 40 kDa for the CA0.5 and 81 kDa for the CA/$CaF_2$0.5 membrane; 10 kDa for the CA2 and 81 kDa for the CA/$CaF_2$2 membrane. For the membranes prepared with a solvent evaporation time of 10 minutes, the introduction of 0.05 wt% of CaF_2 decreases the MWCO from 70 kDa for the CA10 membrane to 51 kDa for the CA/$CaF_2$10 membrane. This indicates that the active layer of the membranes prepared with solvent evaporation times of 30 seconds and 2 minutes containing 0.05 wt.% of CaF_2 is composed of an organic-inorganic network with larger pore sizes which allow the permeation of molecules approximately two times the size of those retained by the membranes composed solely of CA. Further increase in the

solvent evaporation time to 10 minutes has the opposite effect: the introduction of CaF_2 decreases the open spaces between the organic-inorganic networks compared to the pure CA membrane (MWCO 70 kDa), inhibiting the permeation of molecules with molecular weights higher than 51 kDa. The change in the structure of the membrane could also be due to the formation of particle agglomerates, since they can possibly act as blocking points for polymers with equal to or greater molecular weight than 51 kDa. Therefore, it would be important to use another casting solution composition, or another stabilizer for the fluorite particles, in order to avoid the cluster formation due to agglomeration.

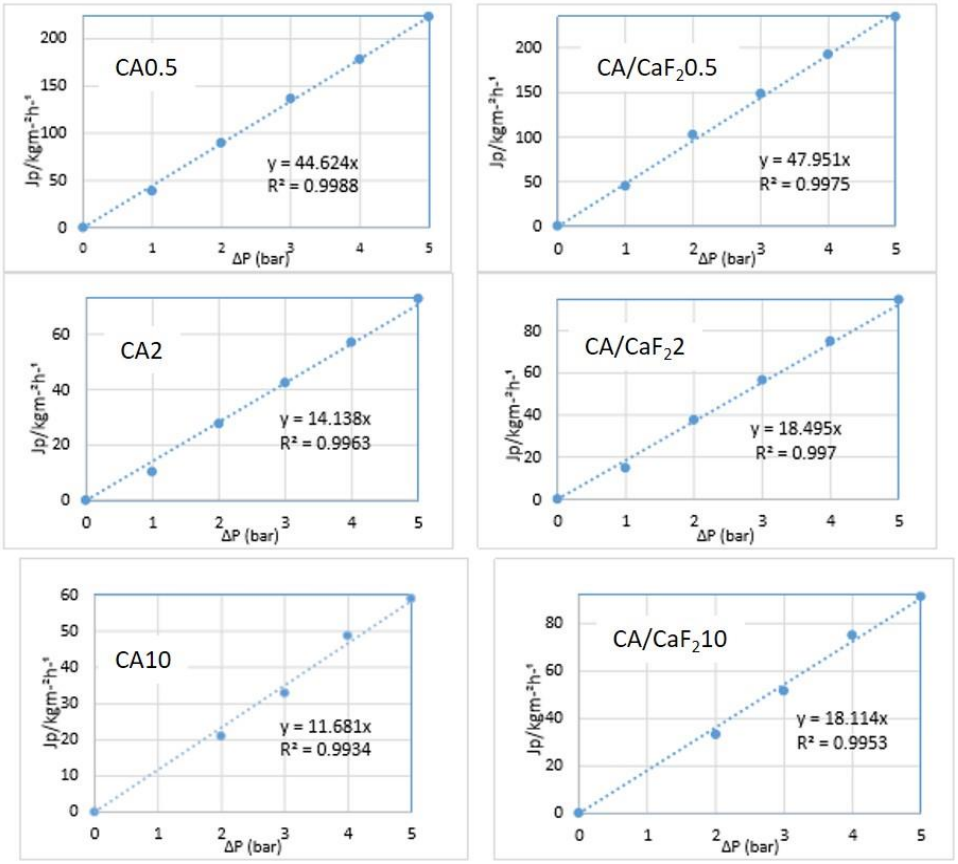

Fig. 10. Variation of the pure water permeation fluxes with the transmembrane pressure for the CA membranes (first column) and the CA/CaF_2 composite membranes (second column) with solvent evaporation times of 0.5 min (row 1), 2 min (row 2), and 10 min (row 3). The hydraulic permeability, L_p, is given by the slope of each curve.

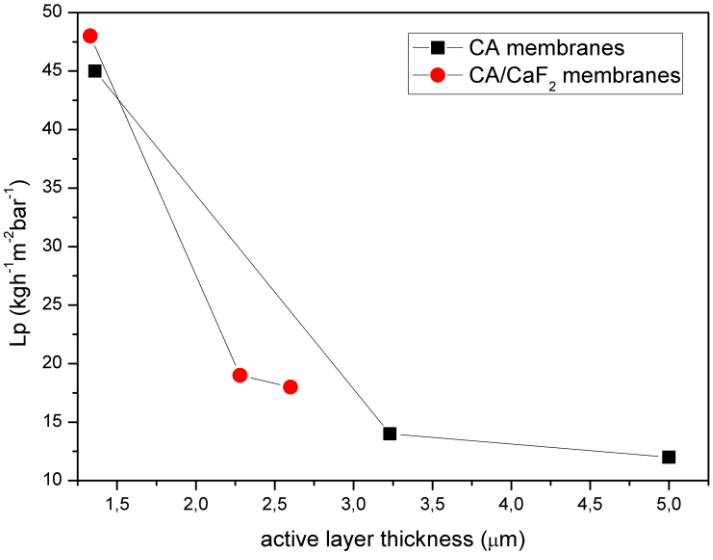

Fig. 11. Hydraulic permeability, L_p, as a function of the active layer thickness for the CA (black square) and CA/CaF_2 composite (red circle) membranes.

4. Conclusions

The synthesis of CA/CaF_2 asymmetric composite membranes results in the ordering of the polymer matrix and, therefore, in different permeation properties. There is an increase in the hydrodynamic permeabilities of the CA/CaF_2 membranes when compared to the corresponding CA membranes. In terms of the MWCO, the incorporation of 0.05 wt.% of CaF_2 increases the value of the MWCO in the membranes prepared with a solvent evaporation time of 0.5 and 2 min: 40 kDa for the CA0.5 and 81 kDa for the CA/$CaF_2$0.5 membrane; 10 kDa for the CA2 and 81 kDa for the CA/$CaF_2$2 membrane. For the membranes prepared with a solvent evaporation time of 10 minutes, the introduction of 0.05 wt% of CaF_2 decreases the MWCO from 70 kDa for the CA10 membrane to 51 kDa for the CA/$CaF_2$10 membrane.

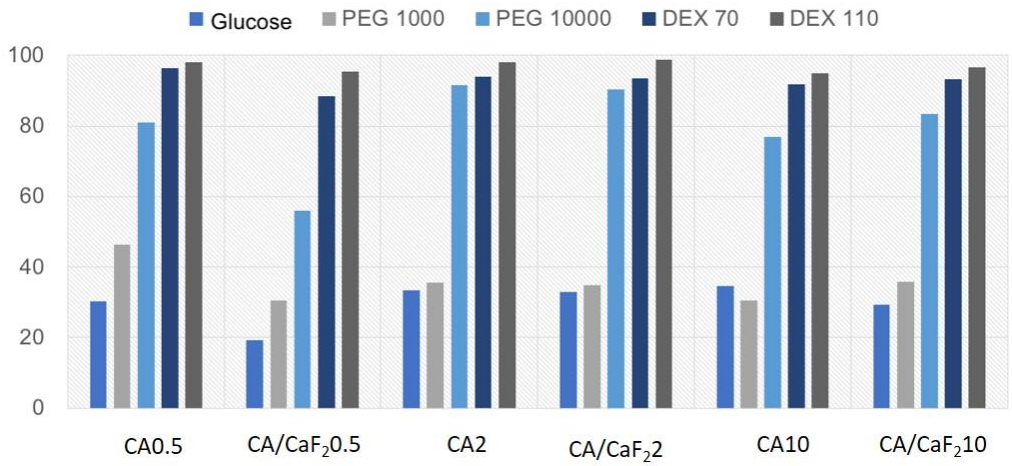

Fig. 12. Membrane rejections to glucose, PEG 1,000 Da, PEG 10,000 Da, Dextran 70,000 Da (DEX 70), Dextran 110,000 Da (DEX 110) for the CA0.5, CA/$CaF_2$0.5, CA2, CA/$CaF_2$2, CA10, and CA/$CaF_2$10 membranes.

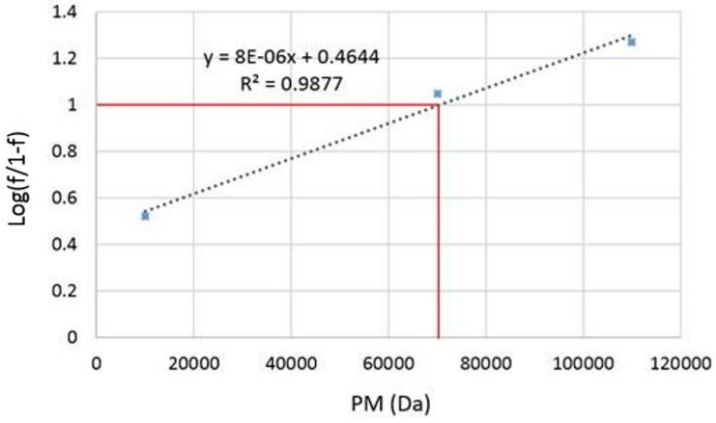

Fig. 13. Determination of the MWCO of the CA10 membrane. Intersection of the two straight lines: $\log\frac{f}{1-f}$ vs MW and $\log\frac{f}{1-f} = 1$.

Acknowledgements

We thank M.M.I.M. Rosa Lina Tovar Tovar (Instituto de Metalurgia/UASLP) for the invaluable help during XRD characterization. The present work was funded by FCT through UID/QUI/00100/2013 and PTDC/CTM-BIO/6178/2014 project and CeFEMA through UID/CTM/04540/201. Andrea Molina thanks Consejo Nacional de Ciencia y Tecnología (CVU 638408) for the financial support during the graduate program in SLP, and the stay at the IST.

References

[1] R.J. Sánchez-Leija, M. Riba-Moliner, D. Cayuela-Marín, O. Domínguez-Espinós, M.G. Sánchez-Loredo, Surface effect of two different calcium fluoride fillers on the non-isothermal crystallization behavior of poly(ethylene terephthalate), J. Macromol. Sci. B 53 (2014) 173–190. https://doi.org/10.1080/00222348.2013.810046.

[2] R.J. Sánchez-Leija, M. Riba-Moliner, D. Cayuela-Marín, O. Domínguez-Espinós, M.G. Sánchez-Loredo, Surface modification of a calcium fluoride filler and the effect on the nonisothermal crystallization behavior of poly(ethylene terephthalate), Polym. Eng. Sci. 54 (2014) 2938–2946. https://doi.org/10.1002/pen.23855.

[3] S. Sathyamurthy, E. Tuncer, K.L. More, B. Gu, I. Sauers, M.P. Paranthaman, Colloidal synthesis of BaF_2 nanoparticles and their application as fillers in polymer nanocomposites, Appl. Phys. A. 106 (2012) 661–667. https://doi.org/10.1007/s00339-011-6652-1.

[4] S.G. Lee, J.-W. Ha, E.-H. Sohn, I.J. Park, S.-B. Lee, Enhancement of polar crystalline phase formation in transparent PVDF-CaF_2 composite films, Appl. Surf. Sci. 390 (2016) 339–345. https://doi.org/10.1016/j.apsusc.2016.08.090.

[5] C. Fritz, Synthesis of nanocomposite materials of magnesium fluoride in polymers, Humboldt University, Berlin, Germany, 2008.

[6] W.A. Bala, V.S. Benitha, K. Jeyasubramanian, G.S. Hikku, P. Sankar, S.V. Kumar, Investigation of anti-bacterial activity and cytotoxicity of calcium fluoride nanoparticles, J. Fluorine Chem. 193 (2017) 38–44. https://doi.org/10.1016/j.jfluchem.2016.11.014.

[7] B. Paosawatyanyong, T. Supasai, V. Pavarajarn, S.K. Hodak, Hydrophobicity improvement of PET fabrics after SF6 plasma treatment, IPP 23 (2008) 135–139. https://doi.org/10.3139/217.2015.

[8] L. Cheng, M.D. Weir, H.H.K. Xu, A.M. Kraigsley, N.J. Lin, S. Lin-Gibson, X.

Zhou, Antibacterial and physical properties of calcium-phosphate and calcium-fluoride nanocomposites with chlorhexidine, Dent. Mater. 28 (2012) 573–583. https://doi.org/10.1016/j.dental.2012.01.006.

[9] M. Łukomska-Szymańska, B. Zarzycka, J. Grzegorczyk, K. Sokołowski, K. Półtorak, J. Sokołowski, B. Łapińska, Antibacterial properties of calcium fluoride-based composite materials: In Vitro study, BioMed Res. Int. (2016). https://doi.org/10.1155/2016/1048320.

[10] A.S. Figueiredo, A.R. Garcia, M. Minhalma, L. Ilharco, M. de Pinho, The ultrafiltration performance of cellulose acetate asymmetric membranes: A new perspective on the correlation with the Infrared Spectra, J. Membr. Sci. Res. 6 (2020) 70–80. https://doi.org/10.22079/jmsr.2019.110424.1269.

[11] M. Faria, C. Moreira, T. Eusébio, P. Brogueira, M.N. de Pinho, Hybrid flat sheet cellulose acetate/silicon dioxide ultrafiltration membranes for uremic blood purification, Cellulose (2020). https://doi.org/10.1007/s10570-020-02985-2.

[12] G. Mendes, M. Faria, A. Carvalho, M.C. Gonçalves, M.N. de Pinho, Structure of water in hybrid cellulose acetate-silica ultrafiltration membranes and permeation properties, Carbohydr. Polym. 189 (2018) 342–351. https://doi.org/10.1016/j.carbpol.2018.02.030.

[13] A. Safronikhin, H. Ehrlich, G. Lisichkin, Double-jet precipitation synthesis of CaF_2 nanoparticles: The effect of temperature, solvent, and stabilizer on size and morphology, J. Alloys Compd. 694 (2017) 1182–1188. https://doi.org/10.1016/j.jallcom.2016.10.128.

[14] B. Kunst, S. Sourirajan, An approach to the development of cellulose acetate ultrafiltration membranes, J. Appl. Polym. Sci. 18 (1974) 3423–3434. https://doi.org/10.1002/app.1974.070181121.

[15] M.D. Afonso, M.N. De Pinho, Ultrafiltration of bleach effluents in cellulose production, Desalination 79 (1990) 115–124. https://doi.org/10.1016/0011-9164 (90) 85001-Q.

[16] A. Taylor, X-ray metallography, John Wiley & Sons, New York, 1961.